International Journal of Physical Sciences

Volume 10 Number 14 30 July, 2015

ISSN 1992-1950

Academic Journals

ABOUT IJPS

The **International Journal of Physical Sciences (IJPS)** is published weekly (one volume per year) by Academic Journals.

International Journal of Physical Sciences (IJPS) is an open access journal that publishes high-quality solicited and unsolicited articles, in English, in all Physics and chemistry including artificial intelligence, neural processing, nuclear and particle physics, geophysics, physics in medicine and biology, plasma physics, semiconductor science and technology, wireless and optical communications, materials science, energy and fuels, environmental science and technology, combinatorial chemistry, natural products, molecular therapeutics, geochemistry, cement and concrete research, metallurgy, crystallography and computer-aided materials design. All articles published in IJPS are peer-reviewed.

Contact Us

Editorial Office: ijps@academicjournals.org

Help Desk: helpdesk@academicjournals.org

Website: http://www.academicjournals.org/journal/IJPS

Submit manuscript online http://ms.academicjournals.me/

Editors

Prof. Sanjay Misra
Department of Computer Engineering, School of Information and Communication Technology
Federal University of Technology, Minna,
Nigeria.

Prof. Songjun Li
School of Materials Science and Engineering,
Jiangsu University,
Zhenjiang,
China

Dr. G. Suresh Kumar
Senior Scientist and Head Biophysical Chemistry
Division Indian Institute of Chemical Biology
(IICB)(CSIR, Govt. of India),
Kolkata 700 032,
INDIA.

Dr. 'Remi Adewumi Oluyinka
Senior Lecturer,
School of Computer Science
Westville Campus
University of KwaZulu-Natal
Private Bag X54001
Durban 4000
South Africa.

Prof. Hyo Choi
Graduate School
Gangneung-Wonju National University
Gangneung,
Gangwondo 210-702, Korea

Prof. Kui Yu Zhang
Laboratoire de Microscopies et d'Etude de Nanostructures (LMEN)
Département de Physique, Université de Reims,
B.P. 1039. 51687,
Reims cedex,
France.

Prof. R. Vittal
Research Professor,
Department of Chemistry and Molecular Engineering
Korea University, Seoul 136-701,
Korea.

Prof Mohamed Bououdina
Director of the Nanotechnology Centre
University of Bahrain
PO Box 32038,
Kingdom of Bahrain

Prof. Geoffrey Mitchell
School of Mathematics,
Meteorology and Physics
Centre for Advanced Microscopy
University of Reading Whiteknights,
Reading RG6 6AF
United Kingdom.

Prof. Xiao-Li Yang
School of Civil Engineering,
Central South University,
Hunan 410075,
China

Dr. Sushil Kumar
Geophysics Group,
Wadia Institute of Himalayan Geology,
P.B. No. 74 Dehra Dun - 248001(UC)
India.

Prof. Suleyman KORKUT
Duzce University
Faculty of Forestry
Department of Forest Industrial Engineeering
Beciyorukler Campus 81620
Duzce-Turkey

Prof. Nazmul Islam
Department of Basic Sciences & Humanities/Chemistry,
Techno Global-Balurghat, Mangalpur, Near District Jail P.O: Beltalapark, P.S: Balurghat, Dist.: South Dinajpur,
Pin: 733103,India.

Prof. Dr. Ismail Musirin
Centre for Electrical Power Engineering Studies (CEPES), Faculty of Electrical Engineering, Universiti Teknologi Mara,
40450 Shah Alam,
Selangor, Malaysia

Prof. Mohamed A. Amr
Nuclear Physic Department, Atomic Energy Authority
Cairo 13759,
Egypt.

Dr. Armin Shams
Artificial Intelligence Group,
Computer Science Department,
The University of Manchester.

Editorial Board

Prof. Salah M. El-Sayed
Mathematics. Department of Scientific Computing.
Faculty of Computers and Informatics,
Benha University. Benha ,
Egypt.

Dr. Rowdra Ghatak
Associate Professor
Electronics and Communication Engineering Dept.,
National Institute of Technology Durgapur
Durgapur West Bengal

Prof. Fong-Gong Wu
College of Planning and Design, National Cheng Kung University
Taiwan

Dr. Abha Mishra.
Senior Research Specialist & Affiliated Faculty.
Thailand

Dr. Madad Khan
Head
Department of Mathematics
COMSATS University of Science and Technology
Abbottabad, Pakistan

Prof. Yuan-Shyi Peter Chiu
Department of Industrial Engineering & Management
Chaoyang University of Technology
Taichung, Taiwan

Dr. M. R. Pahlavani,
Head, Department of Nuclear physics,
Mazandaran University,
Babolsar-Iran

Dr. Subir Das,
Department of Applied Mathematics,
Institute of Technology, Banaras Hindu University,
Varanasi

Dr. Anna Oleksy
Department of Chemistry
University of Gothenburg
Gothenburg,
Sweden

Prof. Gin-Rong Liu,
Center for Space and Remote Sensing Research
National Central University, Chung-Li,
Taiwan 32001

Prof. Mohammed H. T. Qari
Department of Structural geology and remote sensing
Faculty of Earth Sciences
King Abdulaziz UniversityJeddah,
Saudi Arabia

Dr. Jyhwen Wang,
Department of Engineering Technology and Industrial Distribution
Department of Mechanical Engineering
Texas A&M University
College Station,

Prof. N. V. Sastry
Department of Chemistry
Sardar Patel University
Vallabh Vidyanagar
Gujarat, India

Dr. Edilson Ferneda
Graduate Program on Knowledge Management and IT,
Catholic University of Brasilia,
Brazil

Dr. F. H. Chang
Department of Leisure, Recreation and Tourism Management,
Tzu Hui Institute of Technology, Pingtung 926,
Taiwan (R.O.C.)

Prof. Annapurna P.Patil,
Department of Computer Science and Engineering,
M.S. Ramaiah Institute of Technology, Bangalore-54,
India.

Dr. Ricardo Martinho
Department of Informatics Engineering, School of Technology and Management, Polytechnic Institute of Leiria, Rua General Norton de Matos, Apartado 4133, 2411-901 Leiria,
Portugal.

Dr Driss Miloud
University of mascara / Algeria
Laboratory of Sciences and Technology of Water
Faculty of Sciences and the Technology
Department of Science and Technology
Algeria

Prof. Bidyut Saha,
Chemistry Department, Burdwan University, WB,
India

International Journal of Physical Sciences

Table of Contents: Volume 10 Number 14, 30 July, 2015

ARTICLES

Synthesis and magnetic characterization of nanoparticles 413
Enzo Hernández and Vicente Sagredo

Atom-field interaction, hydrogen atom and nature of detuning 420
R. Bora Bordoloi, R. Bordoloi and G. D.Baruah

academicJournals

Vol. 10(14), pp. 413-419, 30 July, 2015
DOI: 10.5897/IJPS2015.4304
Article Number: DE27BD754496
ISSN 1992 - 1950
Copyright ©2015
Author(s) retain the copyright of this article
http://www.academicjournals.org/IJPS

International Journal of Physical Sciences

Full Length Research Paper

Synthesis and magnetic characterization of $ZnMnO_3$ nanoparticles

Enzo Hernández* and Vicente Sagredo

Magnetism Laboratory, Department of Physics, Faculty of Science, 5101 University of Los Andes, Merida, Venezuela.

Received 1 April, 2015; Accepted 26 June, 2015

$Z_nM_nO_3$ nanoparticles system was prepared by the sol-gel auto-combustion method, in order to analyze the structure and magnetic behavior presented in such compound prepared by a new alternative route of synthesis. Structural characterization, bonds, morphology and size were performed by X-ray diffraction (XRD), infrared spectroscopy (IR) and electron microscopy (TEM) and additionally an optical characterization (UV-vis) at room temperature. The XRD study showed that the $ZnMnO_3$ compound crystallized in a mixed cubic perovskite-wurtzite structure. The IR spectra showed that the compound has energy bands in the $Mn-O-Mn$ bonds related with octahedral; which is attributed to a vibration characteristic of the perovskite ABO_3 type, addition to find the absorption bands associated with $Zn-O$ bonds, characteristic of the presence of structural wurtzite hexagonal phase. An estimated size and morphological analysis was carried out by applying the Scherrer´s formula and Transmission Electron Microscopy (TEM), revealing non-spherical nanoparticles of 16nm in size. The magnetic measurements M(T) were performed using zero-field-cooled (ZFC) and field-cooled (FC) protocols revealing a negative Weiss temperature indicating antiferromagnetic behavior with a Néel temperature of 13K. From the optical characterization was possible to get the energy gap at room temperature of $E_g \cong 2{,}21eV$.

Key words: Auto-combustion, antiferromagnetic, manganites, nanoparticles, Néel temperature, perovskite, Sol-Gel, Wurtzite.

INTODUCTION

Crystallographic phases in $Zn-Mn-O$ systems have been report generally in two types, hexagonal $ZnMnO_3$ and tetragonal spinel $ZnMn_2O_4$ (Saraf et al., 2010). $ZnMnO_3$ phase is mostly observed in the form of a phase mixture along with ZnO and $ZnMn_2O_4$ (Saraf et al., 2010; James et al., 2012). There are few reports of successful synthesis approaches towards $ZnMnO_3$ (in the mixed phase form) partly because of its instability; relatively narrower Mn doping and temperature range for $ZnMnO_3$ formation (Peiteado et al., 2007; Chamberland et al., 1970). Tetravalent manganese compounds such as MnO_2 and $AMnO_3$ have been previously reported, while the spinels of $Mn(IV)$ are rare. $AMnO_3$ (A=Ca, Ba, Sr, Ni, Co, Zn and Mg) compounds containing $Mn(IV)$ ions normally crystallize in either the ilmenite (A=Ni, Co, Zn and Mg) or the ABO_3 perovskites structure (A=Ca, Ba and Sr)

*Corresponding author: E-mail: enzovha@gmail.com
Author(s) agree that this article remain permanently open access under the terms of the Creative Commons Attribution License 4.0 International License

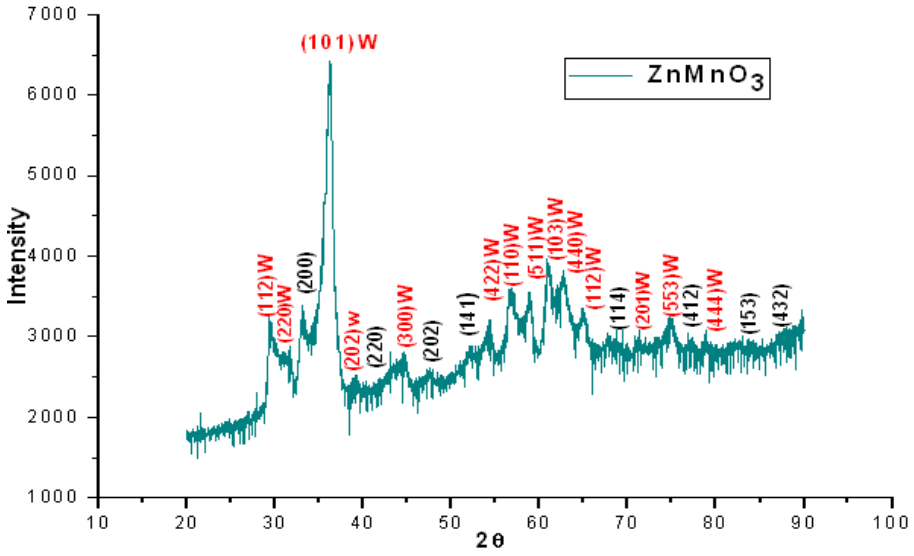

Figure 1. Pattern XRD nanoparticles of $ZnMnO_3$.

(Menaka et al., 2011); in which it can have an ideal structure cubic $P_{m\bar{3}m}$ space group, orthorhombic P_{bnm} space group or rhombohedral $R_{\bar{3}CH}$ space group. The stoichiometry with valence states corresponding to Zinc Manganites $ZnMnO_3$ is $A^{+2}B^{+4}O_3^{-2}$, assigning a cubic unit cell body-centered, bcc, whose center Zn^{+2} cation is placed; Mn^{+4} cations occupying the eight vertices of the cell and the anions bcc O^{-2} occupy the mid-points between the cations B, in the middle of the edges of the bcc cell (Varshney and Kaurav, 2004; Ghosh et al., 2007).

Here the authors present synthesis, X-Ray diffraction (XRD) and magnetic measurements $M(T)$ of the $ZnMnO_3$ nanoparticles system of the mixed cubic structure, perovskite-wurtzita. The results of detailed magnetic $M(T)$ studies show an antiferromagnetic behavior with $T_N = 13K$, behavior reported very recently (Menaka et al., 2011; Jacimovic et al., 2011). Nevertheless, ferrimagnetic behavior has also been reported in $ZnMnO_3$ nanoparticles with a Néel temperature of 20 K (James et al., 2012); in previous years, Saraf et al. (2010) reported sol-gel synthesis of nanoparticles of cubic $ZnMnO_3$ with D = 30 nm as size using nitrates method but without reporting any magnetic investigations. The synthesis of a cubic $ZnMnO_3$ nanoparticles was also reported by Toussaint (1964), but again without magnetic characterization (Toussaint, 1964). Recently, Jacimovic et al. (2011) reported the synthesis of cubic $ZnMnO_3$ nanoparticles by using nitrates, they observed splitting of the zero-field-cooled (ZFC) and field-cooled (FC) magnetization data at 15 K; however, no additional details of its magnetic behavior were reported. Therefore, further research is recommended to fully understand the nature of magnetism in $ZnMnO_3$ nanoparticles.

Synthesis

$ZnMnO_3$ nanoparticles systems were synthesized by the sol-gel auto-combustion method (Seminario, 2012; Munir and Holt, 1987; Chinarro et al., 2005). The precursors used were Manganese (II) Nitrate, $Mn(NO_3)_2.4H_2O$ and Zinc Nitrate, $Zn(NO_3)_2.6H_2O$; both were easily dissolved in distilled water and stirred for 5 minutes at room temperature. On the other hand, citric acid $C_6H_8O_7 - H_2O$ was used as organic fuel (combustion heat of C_h = 18.3 *KJ*, which is easily dissolved in distilled water, stirred at room temperature for 10 min. All solutions were made separately until get a completely clear solution; then they were mixed and kept under stirring of all precursors already dissolved in a beaker on a hotplate at 85°C for 4 h until the final product has a viscous and yellow appearance. After this, the sol-gel product was deposited in a shuttle glass and the center of a tube furnace preheated to 500°C. The furnace is slightly inclined to produce a slight convection that allows the air circulation at the time at which combustion occurs. A few seconds after introducing the sol-gel in oven, violent flames pointing appearance was observed that the self-combustion process had occurred; this releases large amounts of gases. Just when the material stops emitting gases, about 3 min after entering the material in the oven, the furnace was turns off and allowed to cool to room temperature. It is noted that grayish white foam was obtained. The material it was removed from shuttle glass (when there is combustion the material that is out of the shuttle glass is discarded, only material left inside the shuttle glass after combustion is used) and ground gently on agate stone. Thus $ZnMnO_3$ nanoparticles were obtained.

RESULTS AND DISCUSSION

$ZnMnO_3$ nanoparticles were characterized by X-Ray diffraction without further treatment. The diffractogram obtained at room temperature is shown in Figure 1. This was identified as a mixed cubic perovskite-wurtzite structure, where eight perovskite phase peaks are observed; (200), (220), (202), (141), (114), (412) (153)

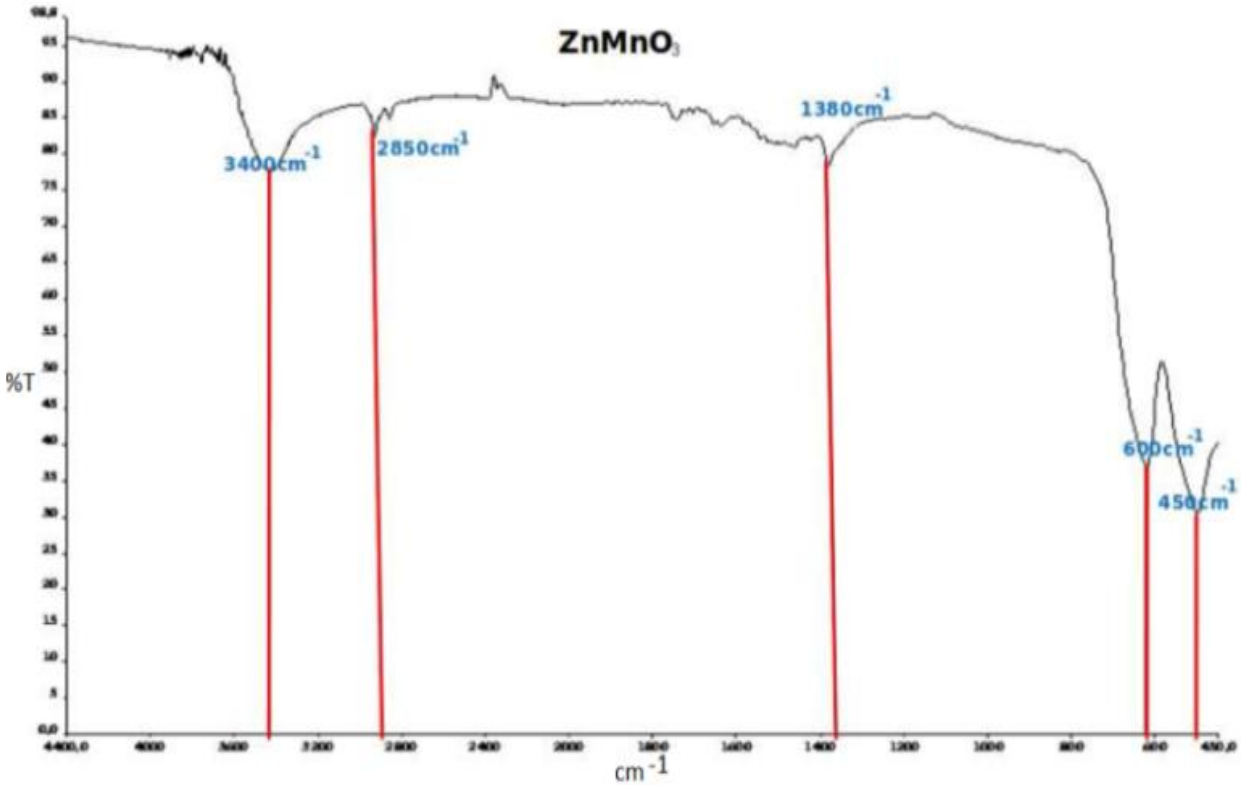

Figure 2. FT-IR spectra for $LaMnO_3$.

and (432) peaks plus fourteen wurtzite phase; (112), (220), (101), (202), (300), (422), (110), (511), (103), (440), (112), (201) (553) and (444). He also proceeded to compare the experimental diffraction pattern with the diffraction pattern of the reference (Saraf et al., 2010) and the JCPDS card #19-1461. Those reports said that the crystal structure of the $ZnMnO_3$ compound is a cubic structure face centered of $P_{m\bar{3}m}$ space group with 8.35 Å and 8.34 Å lattice parameters respectively. For the crystallographic study we use NBS-L program to calculate the value of the lattice parameter, the calculated value was a = 8.3488 Å. By using the diffraction pattern, peak (101), was carried out grain size estimation by applying the Scherrer´s formula to throw a value of $D_S = 18nm$.

Figure 2 shows FT-IR spectra of the $ZnMnO_3$ nanoparticles. In these spectra there are five absorption bands, three around 450, 600 and 3400 cm^{-1} in which the absorption band at 450 cm^{-1} corresponds to the $Zn-O$ bounds, characteristic of the presence of hexagonal wurtzite structural phase. The band at 600 cm^{-1} is attributed to the vibration of $Mn-O-Mn$ bonds perovskite ABO_3 type (Coey et al., 1999; LiK et al., 1997). The absorption band at 3400 cm^{-1} corresponds to $O-H$ stretching vibrations (water). The water present in the samples can result from those compounds are hygroscopic. Finally, two smaller bands around 2850 cm^{-1} corresponding to bonds $C-O_2$, combustion residues and the band at 1380 cm^{-1}, which suggests the presence of *N - o* vibrations could be residues of nitrate source (Wang et al., 2005; Giri et al., 2010; Wade, 2005).

Figure 3 shows an image of $ZnMnO_3$ sample taken with a transmission electron microscope (TEM) with full scale 20 mn. It may be observed that the nanoparticles have an undefined shape (Although micrograph quality could take the necessary information). This is related to the synthesis used, since the self-combustion is not performed in the total thermal equilibrium; the temperature in different parts of the sample to the flame appear at the time of combustion can be quite different, so it may cause a distribution of grain sizes of the obtained material. Attached at the bottom of fig 3 we show the graph of frequency versus particle diameter obtained from $ZnMnO_3$ micrograph, of which was fitted with a Gaussian bell-type displays. This allowed us to estimate an average particle size of $D_{TEM} = 16\ nm$. This value is consistent with Scherrer´s formula value for the size distribution the diameter of about 120 identifiable particles it was measured in the $Z_\eta M_\eta O_3$ micrograph to make a statistical data. The particle sizes were taken by hand using a scale ruler who brings the IMAQ-Vision Builder program that comes with its own micrographs. As the particle shape is not spherical, several measurements of particle diameters (between 4 and 5 values) were

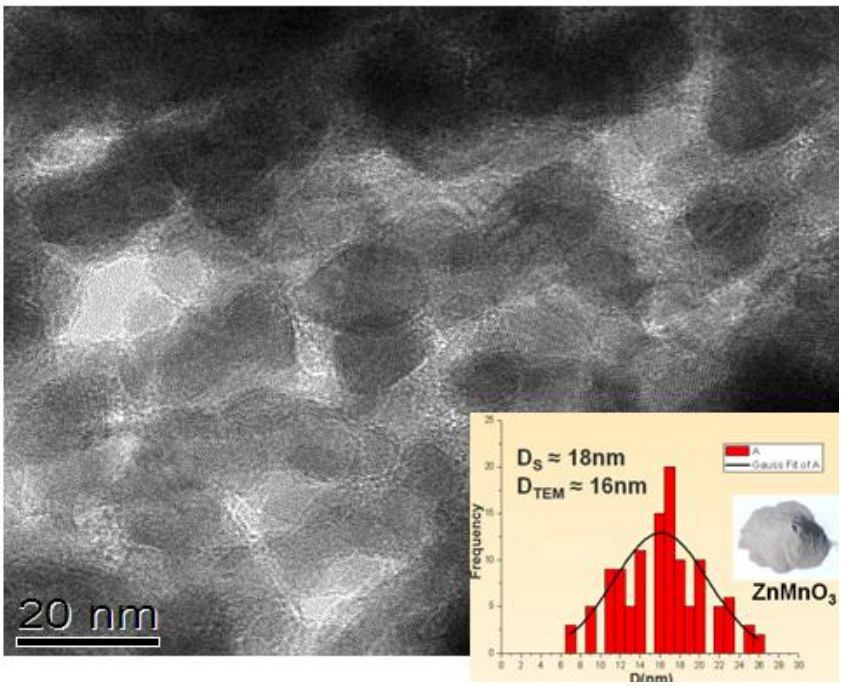

Figure 3. TEM micrographs of $ZnMnO_3$ and size distribution.

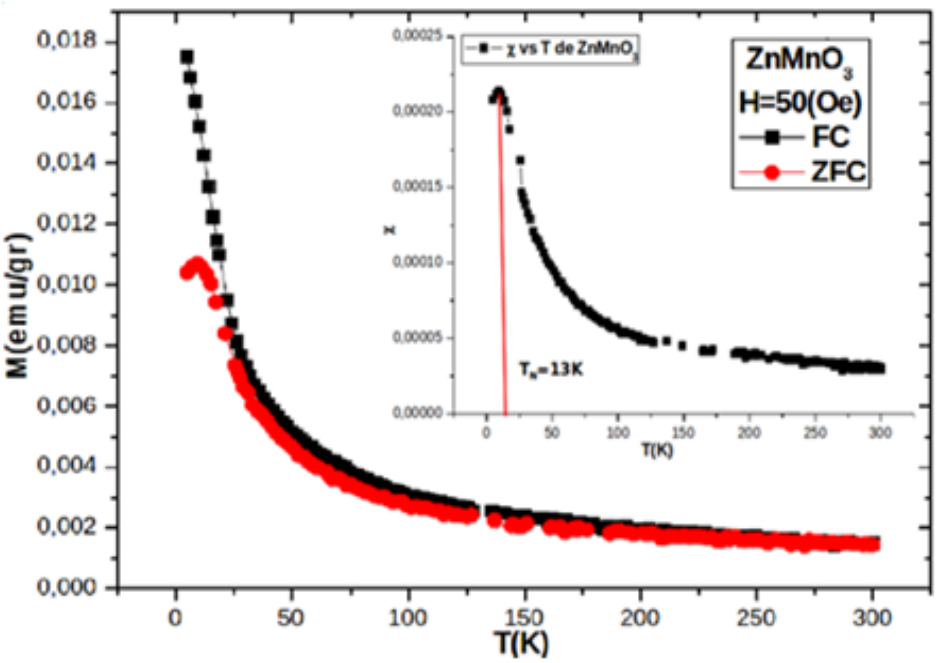

Figure 4. Temperature dependence of the magnetizations for $ZnMnO_3$ nanoparticles.

made to have a simple average for each particle diameter.

Figure 4 shows the $M\ vs\ T$ graph of $ZnMnO_3$ nanoparticles; measured with ZFC and FC protocols in the temperature range of 5 K to 300 K. It can also be observe an irreversibility temperature, T_{irr}, at 160 K. In the ZFC curve a transition zone is observed at low temperatures suggesting that we could be approaching to

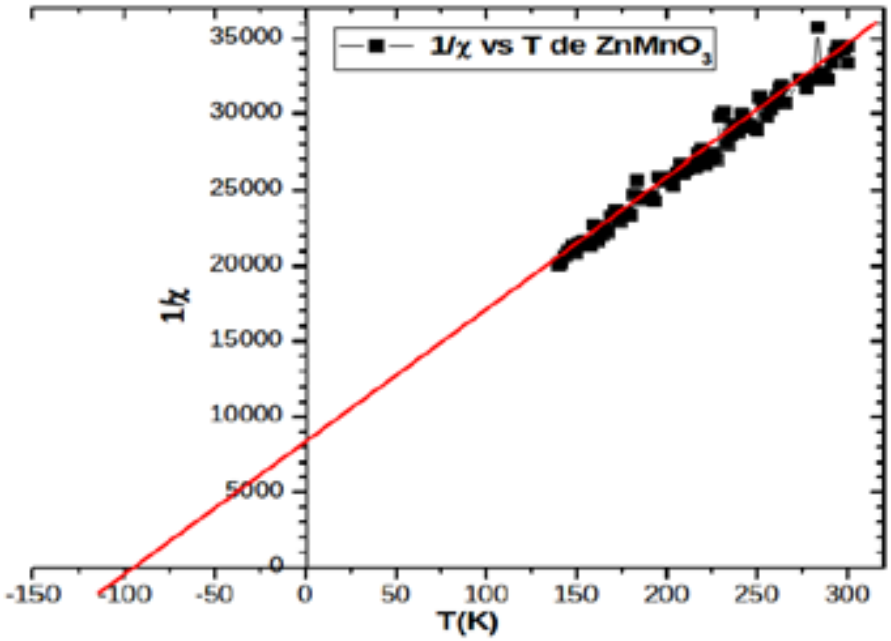

Figure 5. $1/\chi\ vs\ T$ for nanoparticles of $ZnMnO_3$.

some magnetic ordering. The ZFC-FC magnetization curves, presented in fig 4, taken at low temperature, show that there are an AFM transition at 13 K, taken as Neel temperature T_N, see inset of Figure 4, in agreement with previous determination. Notice that for $T \leq T_N$ the curves ZFC and FC are widely separated. In the paramagnetic region, $T \geq T_N$ shown in inset of Figure 4, the magnetic susceptibility; M/H = χ versus temperature follow the Curie-Weiss law: $\chi = C/(T-\theta)$ where the constant C and the paramagnetic Curie temperature θ may be obtained by using the linear behavior presented in fig 5. From the fit of $1/\chi\ vs\ T$ in the range of 130 to 300 K temperature, $\theta = -98\,K$ was obtained.

Figure 5 shows the $1/\chi\ vs\ T$ taken from FC data. The negative value of θ is in agreement with the antiferromagnetic magnetic interaction which is expected in these type of materials $Zn^{+2}Mn^{+4}O_3^{-2}$ (Menaka et al., 2011; Jacimovic et al., 2011); in which Mn has a valence state causing only bounds $Mn^{+4} - O^{-2} - Mn^{+4}$ which show a magnetic super-exchange interaction. The experimental value of the effective magnetic moment obtain from the fit of the constant C was $\mu_{eff-ex} = 3.72\,\mu_B$ which is close to the theoretical value of the effective magnetic momentum $\mu_{eff-teo} = 3.81\,\mu_B$ (Coey et al., 1999; Arbuzova et al., 2008). The small discrepancy between the theoretical value and the experimental effective magnetic moment may be due to the fact that this sample has a mixed perovskite-wurtzite structure; mainly because the presence of wurtzite crystalline phases of ZnO.

Figure 6 shows the UV-vis optical absorption graph of $ZnMnO_3$ nanoparticles. For the optical measurements, a pellet of mass 1.5 g with composition of 90% of $ZnMnO_3$ and 10% KBr make, the pellet is homogeneous in consistency. This mixture was brought into a press with a circular mold where it was subjected to a pressure of $10\,T/cm^2$, obtaining a thickness 0.65 mm pad. The optical absorption spectrum was taken at room temperature. The energy gap value was estimated using the relationship: $\alpha h\nu = A(h\nu - E_g)^{1/2}$. Where $h\nu$ is the photon energy, α is the absorption coefficient, $(\alpha = A_\lambda/d)$, where A_λ is the absorbance and d is the thickness of sample pellet, E_g is the energy gap and A a constant. The direct energy gap can be obtained from the extrapolation of straight line to $(\alpha h\nu) = 0$ as is shown in fig 6. For the UV-vis optical absorption graph analysis measure, the absorption coefficient α, for different nominal values of x was calculated and plotted as a function of incident photon energy (Jacimovic et al., 2011) at room temperature. This shows that there is a region close to a linear behavior in the region between 2.5 eV and 3.5 eV. The main edge is constituted by a $E_g \cong 2.21eV$ direct transition value. Then, the quadratic dependence of the product of the absorption coefficient with the energy of the incident photon is obtained. Before starting with the analysis of the result, we mention that the results obtained for the $ZnMnO_3$ sample is the direct transition analogous to the ZnO; because it has been taken as a reference to ZnO, $Zn_{(1-x)}Mn_{(x)}O$ and $ZnMn_2O_4$ (Pan et al., 2011; Rivas, 2012) in the analysis of optical absorption for zinc manganite $LaMnO_3$, because there are few reports

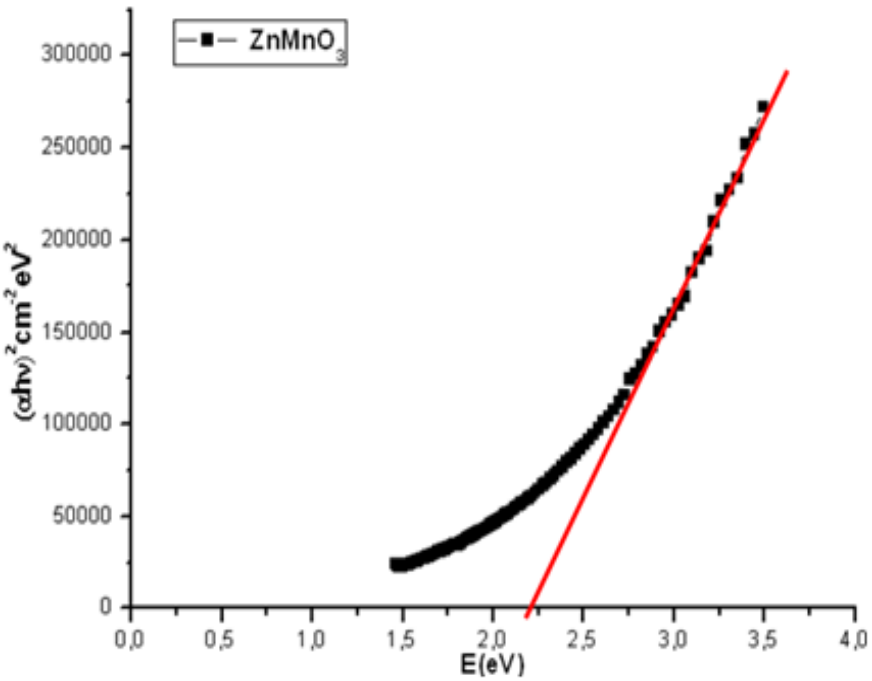

Figure 6. Room temperature at $(\alpha h\nu)^2 vs\, E(h\nu)$.

on the optical absorption of this type of nanoparticles about it. It is assumed that this work is one of the pioneers in the study of the optical absorption of zinc manganite nanoparticles. Considering the reflectivity of the material, with a low absorption of the curve is set to zero, which is a translational axis; furthermore, a high absorption was observed possibly residual defects in the structure of the material, and/or the existence of other phases, etc. Under the experimental conditions which measurements were made, the value of direct energy gap from the reported values regarding Zinc Oxide $E_g \cong 3.40\, eV$ that speak of a decline in the value of the energy gap when the Zinc Oxide is Manganese doped, $Zn_{0,97}Mn_{0.03}O$ in thin films; and in Zinc and Manganese Ferrites, $Mn_{(x)}Zn_{(1-x)}Fe_2O_4$, with a energy gap value about $E_g \cong 2.28eV$; whose values, especially the latter is the closest to those reported in this work (Pan et al., 2011; Rivas, 2012).

CONCLUSIONS AND RECOMMENDATIONS

For the $ZnMnO_3$ as grown nanoparticles we found a mixed cubic perovskite-wurtzite structure *fcc* with lattice parameters $a = 8.3488\,\text{Å}$. FT-IR show the absorptions band at 650 cm^{-1} associated with the perovskites and the absorption band at 450 cm^{-1} corresponding to the ZnO bounds characteristic for the presence of structural wurtzite hexagonal phase; this is consistent with the information obtained from X-ray diffraction. In the $ZnMnO_3$ $M\ vs\ T$ magnetic measurement was found indicating $\theta_w = -98\,K$ antiferromagnetic behavior associated with super exchange interaction, consistent with the majority of reports of such materials; in which Mn has only one valence state. The optical measurements yielded a $E_g \cong 2.21eV$ direct energy value of energy gap. It is recommended to continue the study of the magnetic properties with $M\ vs\ H$ measurements at different temperatures to examine whether there maybe super paramagnetism and $M\ vs\ T$ measurements on alternate fields at different frequencies in a temperature range around the T = 13 K to examine whether some behavior of spin glass is presented and synthesize the $ZnMnO_3$ nanoparticles system following other synthesis methods.

Conflict of Interest

The authors have not declared any conflict of interest.

ACKNOWLEDGEMENTS

The authors are grateful to CDCHTA –ULA for funding the projectC-1658-09-05-A. Also grateful to C. Pernechele and F. Rossi, Dipartamenti di Fisica, CNISM, Universita di Parma, A-1-43100, Italia, and IMEM-CNR Institute, 43019, Parma Italia respectively for experimental collaboration towards the study.

REFERENCES

Arbuzova TI, Gizhevskiĭ BA, Zakharov RG, Petrova SA, Chebotaev NM (2008). Magnetic susceptibility of Nanostructural Manganite $LaMnO_{3+\delta}$ Produced by Mechanochemistry Method. Phys. Solid State 50(8):1487-1494.

Chamberland BL, Sleight AW, Weiher JF (1970). Preparation and Characterization of $MgMnO_3$ and $ZnMnO_3$. J. Solid State Chem. 1:512.

Chinarro E, Chinarro E, Moreno B, Martin D, González L, Villanueva E, Guinea D, Jurado JR (2005). Posibilidades del Análisis de Imagen para el Estudio de la Síntesis de Materiales por Combustión. Bol. Soc. Esp. Ceram. 44(2):105-112.

Coey JMD, Viret M, Von Molnar S (1999). Mixed-Valence Manganites. Adv. Phys. 48:167.

Ghosh S, Sharma AD, Basu RN, Maiti HS (2007). Influence of B Site Substituents on Lanthanum Calcium Chomite Nanocrystalline Materials for a Solid-Oxide Fuel Cell. J. Am. Ceram. Soc. pp. 3741-3747.

Giri A, Makhal A, Ghosh B, Raychaudhuriand AK, Kumar S (2010). Functionalization of manganite nanoparticles and their interaction with biologically relevant small ligands: Picosecond time-resolved FRET studies. Pal. Nanoscale 2:2704-2709.

Jacimovic J, Mickovic Z, Gaal R, Smajda R, Vajie C, Sienkiewicz A, Ferro L, Magrez A (2011). Synthesis, Electrical resistivity, Thermo-Electric Power and Magnetization of Cubic $ZnMnO_3$. Solid State Commun. 151:487.

James DR, Thota S, Kumar J, Seehra MS (2012). Sythesis, Structure and Magnetic Behavior of nanoparticles of Cubic $ZnMnO_3$. Appl. Phys. Lett. 100:252407.

LiK KB, Li XJ, Zhu KG (1997). Infrared Absorption spectra of Manganese Oxides $La_{1-x-y}R_yCa_xMnO_3$. J. Appl. Phys. 10:6943.

Menaka SL, Samal KV, Ramanujachary SE, Lofland G, Ganguli AK (2011). Stabilization of Mn(IV) in Nanostructured Zinc Manganese Oxide and Their Facile Transformation from Nanospheres to Nanorods. J. Mater. Chem. 21:8566.

Munir ZA, Holt JB (1987). The combustion synthesis of refractory nitrides. Theoretical-Analysis. J. Mater. Sci. 22(2):710-714.

Pan Z, Xinyong L, Qidong Z, Shaomin L (2011). Synthesis and optical property of one-dimensional spinel $ZnMn_2O_4$ nanorods. Nanoscale Res. Lett. 6:323.

Pankove J (1971). Optical Processes in Semiconductor. Dover Publications. New York. First Edition.

Peiteado M, Caballero AC, Makovec D (2007). Phase Evolution of $Zn_{1-x}Mn_xO$ system synthesized via oxalate precursors. J. Eur. Ceramic Soc. 27:3915.

Rivas P (2012). Tesis de Lic. En Física. Universidad de los Andes, Venezuela.

Saraf LV, Nachimuthu P, Engelhard M H, Baer DR (2010). Stabilization of $ZnMnO_3$ phase from sol-gel sythesized nitrate precursors. J. Sol-Gel. Sci. Technol. 53:141–147.

Seminario (2012). Métodos de Preparación de nanopartículas. Edgar Pérez, Universidad de los Andes, Mérida Venezuela, 2012.

Toussaint H (1964). Revue de chimie minérale. Revue für anorganische Chemie. Inorganic chemistry review. 1:141.

Varshney D, Kaurav N (2004). Analysis of low temperature specific heat in the ferromagnetic state of the Ca-doped manganites. Eur. Phys. J. B. 37:301-309.

Wade LG (2005). Química Orgánica. 5 edición. http://www.slideshare.net/alis590/quimica-organica-wade-5ta-edicion.

Wang H, Zhao Z, Xu C-M, Liu J (2005). Nanometric $La_{1-x}K_xMnO_3$ Perovskite-type oxides-highly active catalysts for the combustion of diesel soot particle under loose contact conditions. Catal. Lett. 102:5864.

academicJournals

Vol. 10(14), pp. 420-424, 30 July, 2015
DOI: 10.5897/IJPS2015.4302
Article Number: 60C34F554498
ISSN 1992 - 1950
Copyright ©2015
Author(s) retain the copyright of this article
http://www.academicjournals.org/IJPS

International Journal of Physical Sciences

Full Length Research Paper

Atom-field interaction, hydrogen atom and nature of detuning

R. Bora Bordoloi[1]*, R. Bordoloi[2] and G. D.Baruah[2]

[1]Department of Physics, Namrup College, Namrup – 786623, Assam, India.
[2]Center for Laser and Optical Science, New Uchamati, Doom Dooma-786151 India.

Received 27 March, 2015; Accepted 26 June, 2015

The nature of detuning in transition probabilities in atom field interaction has been investigated in the light of hydrogen atom problem. It has been shown that the detuning bears a striking similarity with the principal quantum number *n* in hydrogen atom.

Key words: Induced resonant transition, detuning, hydrogen atom.

INTRODUCTION

Hydrogen atom problem is a well known and simple example of a quantum mechanical system. The solution of the hydrogen atom problem, which gives rise to *principal quantum numbers* and from which we get the energy level diagrams are the basis of all atomic structures (Jenkins and White, 1981). The present investigation is related to the nature of time evolution of the transition probabilities of the interacting two level atoms with a coherent resonant radiation field (Sargent et al., 1974). We have shown that the detuning controlled transition probabilities exhibit a striking similarity with that of the principal quantum number controlled atomic energy level spacing.

HYDROGEN ATOM

In the absence of external forces the classical energy of an electron bound by its negative charge to the positively charged nucleus is given by:

$$\mathrm{H} = \frac{p^2}{2m} - \frac{e^2}{r} \quad (1)$$

Where p, m, e and r have their usual meanings.

The time development of the wave function is determined by the Schrodinger equation.

$$i\hbar\dot{\psi}(\vec{r},t) = H(\vec{r},\vec{p})\psi(\vec{r},t) \quad (2)$$

The Hamiltonian is usually given by classical energy, in which the measurable quantities such as position and momentum are replaced by appropriate operators. The stationary solutions $\psi_n(\vec{r},t)$ of the Schrodinger equation are those for which the time dependence can be separated from the space dependence, that, is for which

$$\psi_n(\vec{r},t) = u_n(\vec{r})\exp\left(-i\omega_n t\right) \quad (3)$$

*Corresponding author. E-mail: rajibassam01@gmail.com
Author(s) agree that this article remain permanently open access under the terms of the Creative Commons Attribution License 4.0 International License

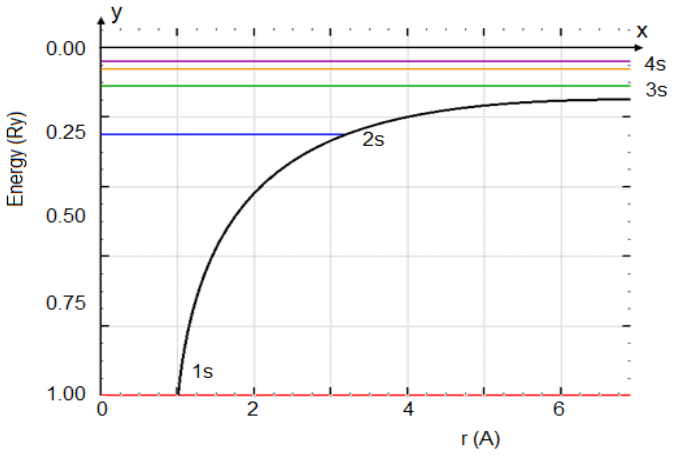

Figure 1. Energy level diagram for hydrogen atom. Horizontal lines indicate energy levels given by Equation (10).

Here ω_n is a circular frequency. Substituting Equation (3) into (2) we find the time-dependent equation

$$H(\vec{r},\vec{p})u_n(\vec{r}) = \hbar\omega_n u_n(\vec{r}) \quad (4)$$

This is an eigen value equation for the Hamiltonian $H(\vec{r},\vec{p})$ with eigen functions $u_n(\vec{r})$ and eigen value $\hbar\omega_n$. The eigen value Equation (4) must be solved for hydrogen atom and then we have

$$\left(\frac{\hbar^2\nabla^2}{2m} - \frac{e^2}{r}\right)u(r) = \hbar\omega u(r) \quad (5)$$

Here it is advantageous to express ∇^2 in spherical coordinates, **r**, and Φ, because of the spherical symmetry of the potential energy $\left(-\frac{e^2}{r}\right)$. The Equation (4) can be separated into three equations, each containing a single spherical coordinate. The solutions of the equations correspond to discrete energies, as for the bound problems and have the values

$$u_{nlm}(r,\theta,\phi) = R_{nl}(r)Y_{lm}(\theta,\phi) \quad (6)$$

Here the $R_{nl}(r)$ are the Laguerre polynomials multiplied by the exponential factor $\exp(-r/na_0), a_0 = 0.53\,\text{Å}$ is the Bohr radius, and $Y_{lm}(\theta,\phi)$ are spherical harmonics. In particular first few $u_{nlm}(r,\theta,\phi)$ are as follows:

$$u_{100}(r,\theta,\phi) = (\pi a_0^3)^{-1/2}\exp(-r/a_0) \quad (7)$$

$$u_{200}(r,\theta,\phi) = (32\pi a_0^3)^{-1/2}(2-r/a_0)\exp(-r/2a_0) \quad (8)$$

$$u_{210}(r,\theta,\phi) = (32\pi a_0^3)^{-1/2}(r/a_0)\cos\theta\exp(-r/2a_0) \quad (9)$$

The corresponding energies are given by

$$\hbar\omega_{nlm} = \hbar\omega_n = \frac{e^2}{2a_0 n^2} \quad (10)$$

Which are discrete, Figure 1 shows the energy level diagram for hydrogen atom worked out with the help of Equation (10).

INDUCED RESONANT TRANSITIONS

Let us now consider our important problem of induced resonant transitions. Specifically consider the hydrogen atom initially in the ground state u_{100}. At time t=0 we apply an oscillating electric field (Sargent et al., 1974).

$$E(t) = \hat{x}E_0\cos\nu t \quad (11)$$

Where

$$\nu \cong (E_2 - E_1)/\hbar \quad (12)$$

Here ν is in radian/sec (not Hertz). The oscillating electric field is nearly resonant with the transitions from *n* =1 to *n* =2. From Figure 2 one can infer that the states u_{nlm} with

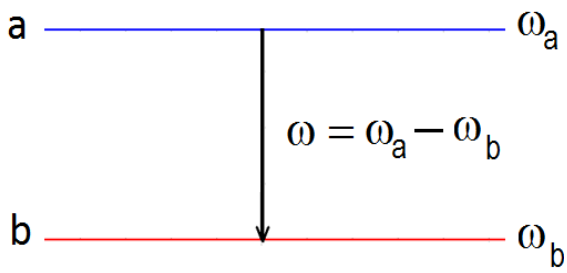

Figure 2. Diagram depicting two energy levels a and b of the unperturbed Hamiltonian.

n>2 are way off resonance with the field incident and therefore can be neglected. Hence we can describe the atom by two level wave function given by:

$$\psi(\vec{r},t) = C_a u_a(\vec{r})\exp(-i\omega_a t) + C_b u_b(\vec{r})\exp(-i\omega_b t) \quad (13)$$

And take the eigen functions

$$u_a = u_{210}$$
$$u_b = u_{100}$$

The coefficients in Equation (13) satisfy the normalization condition

$$|C_a|^2 + |C_b|^2 = 1 \quad (14)$$

The equations of motion for $C_a and C_b$ are given by

$$\dot{C}_a = \frac{1}{2} i\wp \frac{E_0}{\hbar}\left\{\exp\left[i(\omega-\nu)t\right] + \exp\left[i(\omega+\nu)t\right]\right\} C_b \quad (15)$$

$$\dot{C}_b = \frac{1}{2} i\wp \frac{E_0}{\hbar}\left\{\exp\left[-i(\omega-\nu)t\right] + \exp\left[-i(\omega+\nu)t\right]\right\} C_a \quad (16)$$

Where the frequency

$$\omega = \omega_a - \omega_b \quad (17)$$

As shown in Figure 2.

Let us now suppose that the system is in the ground state at time *t*=0, that is, $C_a(0) = 0 \; and \; C_b(0) = 1$, the equation of motion become

$$\dot{C}_b = 0 \quad (18)$$

and

$$\dot{C}_a(0) = \frac{1}{2} i\wp \frac{E_0}{\hbar}\left\{\exp\left[i(\omega-\nu)t\right] + \exp\left[i(\omega+\nu)t\right]\right\} \quad (19)$$

This yield

$$C^{(n)}(t) = \frac{1}{2}\wp \frac{E_0}{\hbar}\left[\frac{\exp\{i(\omega-\nu)t\}-1}{\omega-\nu} + \frac{\exp\{i(\omega-\nu)t\}-1}{\omega+\nu}\right] \quad (20)$$

For optical frequencies the denominator $\omega+\nu$ is very large $(\omega >> 1)$ and therefore the second term in R.H.S. is neglected with respect to the first since at resonance $\omega \cong \nu$.This is called Rotating Wave Approximation (RWA). Thus neglecting the perturbing matrix element is given by:

$$\mathcal{V}_{ab} = -\wp E_0 \cos\nu t = -\wp E_0 \frac{\exp(i\nu t) + \exp(-i\nu t)}{2} \quad (21)$$
$$= -\frac{1}{2}\wp E_0 \exp(-i\nu t) = \mathcal{V}_{ba}$$

Therefore the equations of motion for C_a and C_b under rotating wave approximation become

$$\dot{C}_a = \frac{1}{2} i\wp \frac{E_0}{\hbar}\exp\left[i(\omega-\nu)t\right] C_b \quad (22)$$

$$\dot{C}_b = \frac{1}{2} i\wp \frac{E_0}{\hbar}\exp\left[-i(\omega-\nu)t\right] C_a \quad (23)$$

thus

$$C_a(t) = \frac{1}{2}\frac{\wp E_0}{\hbar}\frac{1}{\omega-\nu}\exp\frac{i(\omega-\nu)t}{2} 2i\sin\frac{(\omega-\nu)t}{2} \quad (24)$$

Thus the probability (Allen and Eberly, 1975) of finding the atom in the upper state is given by

$$|C_a(t)|^2 = C_a(t)C_a(t)^* = \left(\frac{\wp E_0}{2\hbar}\right)^2 \frac{\sin^2\left[(\omega-\nu)t/2\right]}{\left[(\omega-\nu)t/2\right]^2} \quad (25)$$

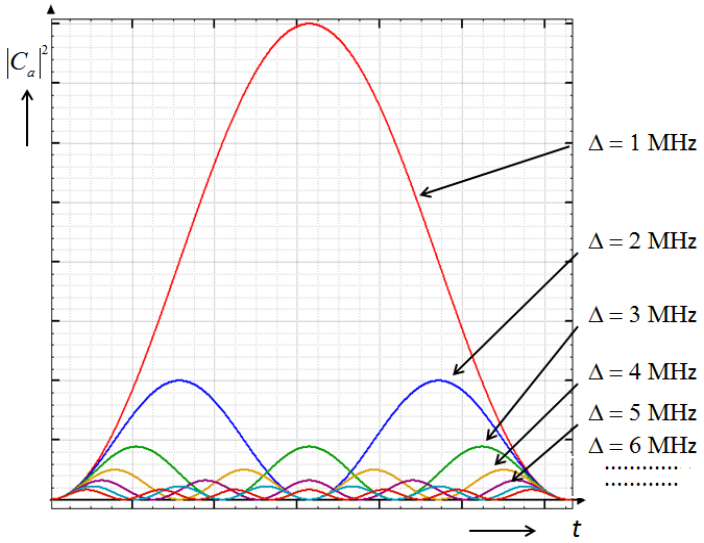

Figure 3. The probability of a transition to an upper level under the influence of an applied electric field.

This is known as stimulated absorption. We could have chosen $C_a(0)=1 \, and \, C_b(0)=0,$ which shows that the atom is initially in the upper state and calculate the probability of stimulated emission. We find in this also the same formula as given by Equation (25). The probability is plotted in Figure 3.

NATURE OF DETUNING

From what has been discussed in the earlier sections it is now appropriate to describe the nature of detuning, $\Delta\omega=\omega-\nu$.Here ω is the atomic line center frequency and ν is the laser oscillation frequency in radian/sec. As ν increases (or decreases) from the atomic line center frequency ω, the atomic system goes away from resonance. In Figure 3 we have depicted the transition probabilities versus time at different values of detuning. The salient feature of this figure is that if we draw horizontal lines joining the maxima of the transition probabilities for detunings corresponding to integral values of $\Delta\omega$ we obtain a series of horizontal lines with relative separations, the reverse of which shows striking similarity with the Energy level diagram of the Hydrogen atom.

Figure 4a indicates the horizontal lines thus generated in a reverse way. Figure 4b shows the corresponding energy levels for hydrogen atom as illustrated in Figure 1. The energy level separation of hydrogen atom goes on decreasing as principal quantum number n increases up to ionization limit. This is also observed in Figure 4a, where it is seen that as detuning increases the relative separation decreases. At higher values of detuning the separation of the horizontal lines become extremely small, this is quite similar to the energy levels of hydrogen atom near ionization limit. It is reasonable to explore the physical consequences of the similarity as describe above. The energy level diagram in hydrogen atom is drawn according to energy in Rydberg (Ry). Likewise the horizontal lines in Figure 4a are arranged according to frequency (in Mz). We must note here that the transition probability $|C_a(t)|^2 \, or \, |C_b(t)|^2$ was worked out on the basis of a two body problem or a two level atom. At time *t* = 0 we applied an electric field which is resonant (or nearly resonant) with the transition from *n* = 1 to *n* = 2. Our work is based on the idea that the detuning has a range of values corresponding to 1, 2, 3….etc (in Mz). It is a matter of common experience that the spectral lines (cm^{-1}) corresponding to a particular series (say Balmer series) is precisely obtained by manipulating the principal quantum number n. Thus the transition probabilities at different values of detuning are the manifestation of an atomic structure in general. This observation is expected to draw light in laser physics particularly in atom field interaction. In this connection it is appropriate to recall the statements by Jenkins and White (1981) who indicates the importance of the horizontal lines as energy levels. According to them the importance of this type of diagram is two fold: (1) regardless of the atomic model presented, whether it is an orbital model or any other yet to be proposed in the future, like a quantum mechanical wave model, it represents with high degree of precession the stationary energy states of atom; and (2) it represents the well established law of conservation of energy as applied through Bohr's third postulate. We thus reasonably conclude that our work concerning the

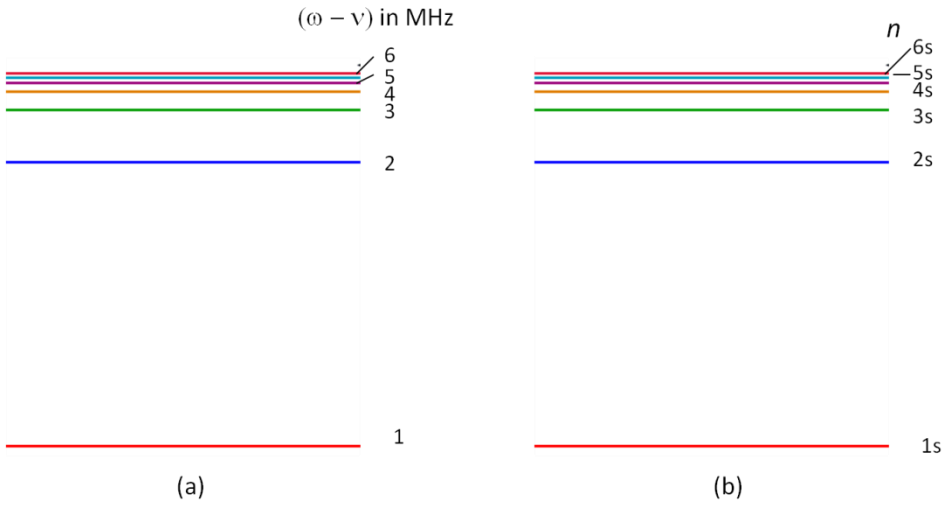

Figure 4. (a) Relative separations of the horizontal lines generated by joining the maxima of the transition probabilities at different detuning (b) Energy levels of hydrogen atom showing relative separations of the principal quantum numbers.

horizontal lines drawn by joining the maxima of the transition probabilities at different values of detuning (ω-ν = 1, 2, 3, ….) only justifies the energy level diagram scheme being introduced more than hundred years ago.

CONCLUSION

In the present work it has been shown that the so called detuning ((ω-ν) bear a striking similarity with the principal quantum number “n” and hydrogen atom. We reasonably conclude that in the present work concerning the horizontal lines joining the maxima of transition probabilities at different values of detuning ((ω-ν = 1,2,3..) only justifies the energy level diagram scheme being introduced more than hundred years ago.

Conflict of Interest

The authors have not declared any conflict of interest.

REFERENCES

Allen L, Eberly J (1975). Optical Resonance and Two level atoms. Wiley Int. Sci. London.

Jenkins FA, White HE (1981). Fundamentals of Optics, Mc GRAW-HILL International Editions, Mc GRAW-HILL Book Company.

Sargent M, Scully MO, Lamb Jr, WE (1974). Laser Physics, (Addison Wesley, New York, 1974).

International Journal of Physical Sciences

Related Journals Published by Academic Journals

- *African Journal of Pure and Applied Chemistry*
- *Journal of Internet and Information Systems*
- *Journal of Geology and Mining Research*
- *Journal of Oceanography and Marine Science*
- *Journal of Environmental Chemistry and Ecotoxicology*
- *Journal of Petroleum Technology and Alternative Fuels*

academicJournals